Journal of Alloys and Compounds 772 (2019) 775–781

Contents lists available at ScienceDirect

Journal of Alloys and Compounds

journal homepage: http://www.elsevier.com/locate/jalcom

Effect of Sc addition, friction stir processing, and T6 treatment on the damping and mechanical properties of 7055 Al alloy

C.Y. Liu [a, b], B. Zhang [c], Z.Y. Ma [a, *], H.J. Jiang [b], W.B. Zhou [d]

[a] Institute of Metal Research, Chinese Academy of Sciences, 72 Wenhua Road, Shenyang 110016, China
[b] Key Laboratory of New Processing Technology for Nonferrous Metal & Materials, Ministry of Education, Guilin University of Technology, Guilin 541004, China
[c] State Key Laboratory of Metastable Materials Science and Technology, Yanshan University, Qinhuangdao 066004, China
[d] Guangxi Pingguo Baikuang High-tech Aluminum Co. LTD, Pingguo 531400, China

ARTICLE INFO

Article history:
Received 15 May 2018
Received in revised form
7 September 2018
Accepted 11 September 2018
Available online 12 September 2018

Keywords:
Al alloy
Microstructure
Damping capacity
Mechanical properties

ABSTRACT

Sc addition, friction stir processing (FSP), and subsequent solid-solution treatment and aging to peak hardness (T6 treatment) were applied on a 7055 Al alloy. Fine equiaxed grains were obtained after FSP, and the size of the grains was further refined by minor Sc addition. Subsequent solid-solution treatment led to the dissolution of η phase, and aging led to the precipitation of η′ phase in the FSP samples. The $Al_3(Sc,Zr)$ particles effectively inhibited the grain coarsening in the Sc-containing FSP sample during the T6 process. Thus, a high density of η′ phase and a fine equiaxed grain structure were obtained in the Sc-containing 7055 alloy after FSP and T6 treatment. The special structure endowed this alloy with higher yield strength than the T6 treated 7055 alloy. FSP enhanced the high-temperature internal friction value of the Sc-containing 7055 alloy, and subsequent T6 treatment did not significantly reduce the value. The Sc-containing 7055 alloy exhibited greater high-temperature internal friction value than the T6 samples and the 7055 alloy fabricated using the same processing route.

1. Introduction

Metallic materials with low density, high strength as well as excellent ductility and damping capacity have attracted considerable attention in modern aerospace industry [1]. Al alloys are important light structural materials with high strength and excellent ductility. However, the poor damping capacity of commercial Al alloys limits their application in aerospace engineering.

Several methods, such as introduction of macroscopic pores [2], high-density of particles with high damping capacity [3–5], and Zn phase [6–9] into Al matrices, have been employed to enhance the internal friction (IF), which is regarded as the damping capacity, of Al alloys. However, the enhancement of IF with the above methods is often detrimental to the mechanical properties.

In our previous investigation, friction stir processing (FSP) based on friction stir welding (FSW) [10–12] was used to enhance the IF of 6082 alloy. The high IF of this FSP sample can be mainly attributed to its equiaxed ultra-fine grain structure. Furthermore, FSP also improves the mechanical properties of the 6082 alloy. However, the strength of the 6082 base metal and FSP 6082 are rather low, with ultimate tensile strength (UTS) of less than 170 MPa [13].

High-strength 7055 alloy is widely used in the modern aerospace industry has also been subjected to FSP to enhance its IF. However, the strength of the 7055 alloy is seriously deteriorated by FSP, although the average grains size (AGS) of the FSP sample is much lower than that of their base metal [14]. The temperature in the stirred zone can reach to as high as 750 K during FSP or FSW [11], and the transformation of η′ into η phase is almost inevitable in the age-hardened 7xxx Al alloys during these processes [15]. The net effect of softening by the disappearance of metastable η′ phase and the hardening by grain refinement result in a decrease in strength [14].

Solid-solution treatment and aging to peak hardness (T6 treatment) could lead to the dissolution of the steady phase and precipitation of metastable phase in the FSP Al alloys, thereby improving their mechanical properties. However, the coarsening of the equiaxed ultra-fine grains after high-temperature solid-solution treatment will decrease the IF value of the FSP samples. Thus, inhibition of grain coarsening of the FSP samples during T6 process may produce Al alloys with high IF value and excellent mechanical

* Corresponding author.
E-mail address: zyma@imr.ac.cn (Z.Y. Ma).

https://doi.org/10.1016/j.jallcom.2018.09.109
0925-8388/

properties.

The $Al_3(Sc,Zr)$ phase with grain boundary (GB) pinning effect in Al alloys could precipitate in Al alloys that contain rare-earth Sc element [16–19]. Thus, the fine grains in the FSP Sc-containing Al alloys may be preserved after heat treatment, such as T6 treatment. Furthermore, Sc addition decreases the AGS of Al alloys during deformation, such as hot rolling [20], hot extrusion [21], and FSP [22–26]. Thus, a high density of η' precipitates and a fine grain structure could be obtained in the FSP 7xxx Al alloys after Sc addition, FSP, and subsequent T6 treatment.

In the present study, 7055 and 7055 + 0.25Sc Al alloys were subjected to FSP and T6 treatment to fabricate 7xxx Al alloys with both high IF value and desirable mechanical properties.

2. Experimental

This study used 3 mm-thick 7055 (7.82 Zn, 1.95 Mg, 2.24 Cu, 0.16Zr) and 7055 + 0.25Sc (7.81 Zn, 1.93 Mg, 2.24 Cu, 0.16Zr, 0.25Sc) alloy sheets. The sheets were solid-solution treated at 743 K for 2 h, and then three routes were implemented: (i) artificial aging at 393 K for 72 h (the sample with peak value was defined as T6 sample); (ii) FSP at a tool rotation rate of 300 rpm, and a traverse speed of 100 mm min^{-1} (defined as FSP sample); and (iii) FSP samples that were solid-solution treated at 743 K for 2 h and then aging at 393 K from for 72 h (the sample with peak value was defined as FSP+T6 sample).

Electron backscatter diffraction (EBSD) and transmission electron microscopy (TEM) were employed to examine the microstructures of the samples. The microstructural examination was performed on the FSP direction–normal direction plane for the FSP and FSP+T6 samples and rolling direction–normal direction plane for the T6 samples. EBSD specimens were mechanically polished, and then electrolytically polished in a solution of 10% perchloric acid and 90% alcohol at 20 V in room temperature. EBSD analysis was performed using a Hitachi S3400N scanning electron microscope coupled with an EDAX EBSD system at an operating voltage of 20 kV and a working distance of 15 mm. TEM specimens were polished to a thickness of 50 μm and then thinned by using a twinjet electropolishing device in a solution of 10% perchloric acid and 90% methanol at room temperature. TEM images were obtained using a JEOL-2010 TEM at 200 kV.

Vickers microhardness of aged samples was measured by EVERONE VH-5 hardness tester with a loading force of 9.8 N for 10 s loading time. Each value in the aging hardness curve was determined by 20 measurements. An Instron-3369-type testing machine was used to evaluate the tensile properties of the samples. The tensile specimens were machined along the FSP direction for the FSP and FSP+T6 samples, and along the rolling direction for the T6 samples. The strain rate of tensile tests was 4×10^{-4} s^{-1}.

A Q800-TA dynamic mechanical analyser was used to evaluate the loss tangent ($\tan\varphi$) of the samples, and the specimens were machined to dimensions of 25 mm × 4 mm × 1.2 mm. The strain amplitude (ε), frequency (f), temperatures (T) and heating rate of the IF tests were 1×10^{-4}, 1 Hz, ranging from 320 K to 653 K, and 5 K/min, respectively. The IF, which is denoted as Q^{-1} [27], for the vibrations is equal to $\tan\varphi$ [28].

3. Results

Fig. 1 shows the aging hardness curves of samples with or without FSP. The samples without FSP exhibited a peak-aged time of 25 h, which was higher than that of FSP samples (12 h). The 7055 + 0.25Sc alloy showed higher hardness value than the 7055 alloy for each parameter. For the alloy with same components, the T6 sample (7055 and 7055 + 0.25Sc with aging 25 h at 393 K) exhibited higher hardness than the FSP+T6 sample (FSP 7055 and 7055 + 0.25Sc with aging 12 h at 393 K).

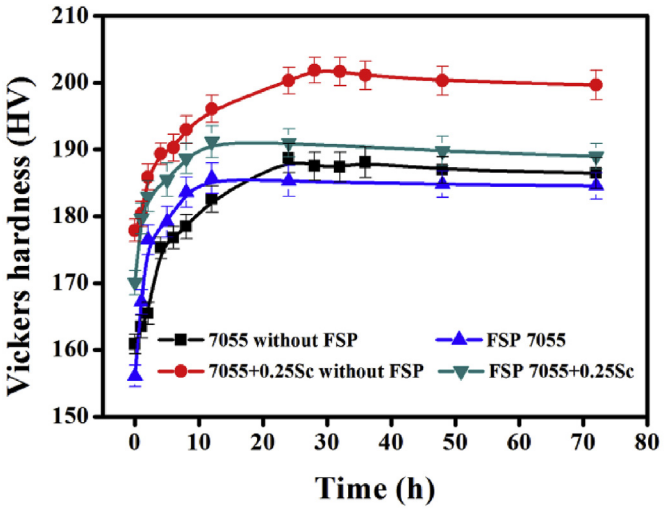

Fig. 1. Aging hardness curves of samples with or without FSP at 393 K.

Fig. 2 shows the EBSD orientation maps of 7055 and 7055 + 0.25Sc alloys. Both fine equiaxed and elongated deformed grains were observed in the T6 samples, and the grains were significantly refined after Sc addition (Fig. 2(a) and (d)). The equiaxed grains were observed in the FSP samples (Fig. 2(b) and (e)), and an additional T6 treatment led to the recrystallized grains coarsening in these FSP samples (Fig. 2(c) and (f)). The FSP+T6 7055 + 0.25Sc sample exhibited a much lower grain size than the 7055 sample under the same heat treatment parameter. However, some significantly coarsened grains, with sizes of 20 μm–50 μm, could be observed in the FSP 7055 + 0.25Sc sample that underwent T6 process (Fig. 2(f)), indicating that local abnormal grain growth occurred during T6 heat treatment.

Fig. 3 shows the inverse pole figures of 7055 + 0.25Sc samples. The strong ⟨111⟩ and ⟨101⟩ texture were the typical texture components for the T6 sample, and this sample exhibited higher maximum texture intensity than the other two samples (Fig. 3(a)). The FSP sample exhibited strong ⟨111⟩ texture and weak ⟨101⟩ texture (Fig. 3(b)). T6 treatment weakened the ⟨111⟩ texture of the FSP sample, but slightly enhanced the ⟨001⟩ texture intensity (Fig. 3(c)).

Fig. 4 shows the distributions of grain size in the FSP and FSP+T6 samples obtained by EBSD. The proportion of large grains (>5 μm) in the 7055 + 0.25Sc alloy was lower than that for the 7055 alloy with the same state. The AGS of the FSP 7055 + 0.25Sc sample was 1.6 μm (Fig. 4(b)), which was smaller than that of the FSP 7055 sample (2.6 μm) (Fig. 4(a)). The AGS of the FSP+T6 7055 sample was 30 μm, and some grains in this sample reached as high as 120 μm (Fig. 4(c)). The AGS of the FSP 7055 + 0.25Sc sample after T6 process was 4.1 μm (Fig. 4(d)).

Fig. 5 shows the misorientation angle distribution of 7055 and 7055 + 0.25Sc samples, and the misorientation angle smaller than 3 was excluded. For the two alloys, the T6 samples exhibited higher fraction of low misorientation angle, and 5.8° was the highest frequency of misorientation angle in these two samples. The FSP and FSP+T6 samples exhibited similar misorientation distribution trend, and the highest frequency of misorientation angle in these samples was 44°.

Fig. 6 shows the TEM images of the 7055 and 7055 + 0.25Sc alloys. The two T6 samples exhibited a high density of precipitates with several nanometres (Fig. 6(a) and (d)). The $Al_3(Sc,Zr)$ particles

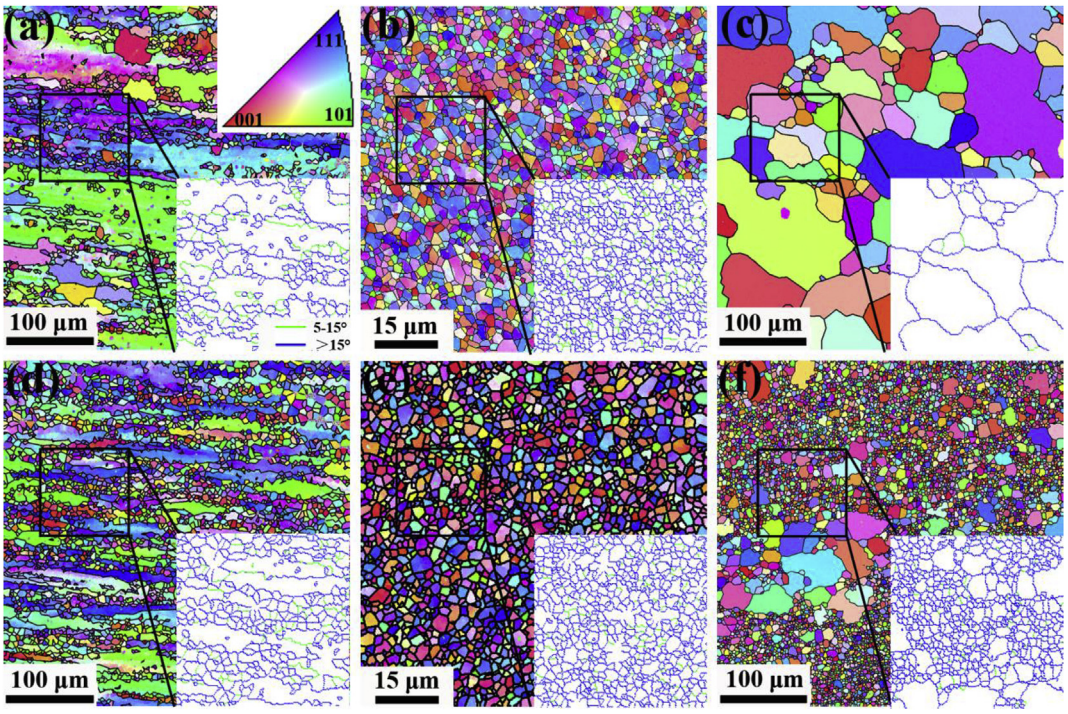

Fig. 2. EBSD orientation maps of (a) T6 7055, (b) FSP 7055, (c) FSP+T6 7055, (d) T6 7055 + 0.25Sc, (e) FSP 7055 + 0.25Sc, and (f) FSP+T6 7055 + 0.25Sc samples. The insert maps are the enlarged view of grain boundaries (GBs).

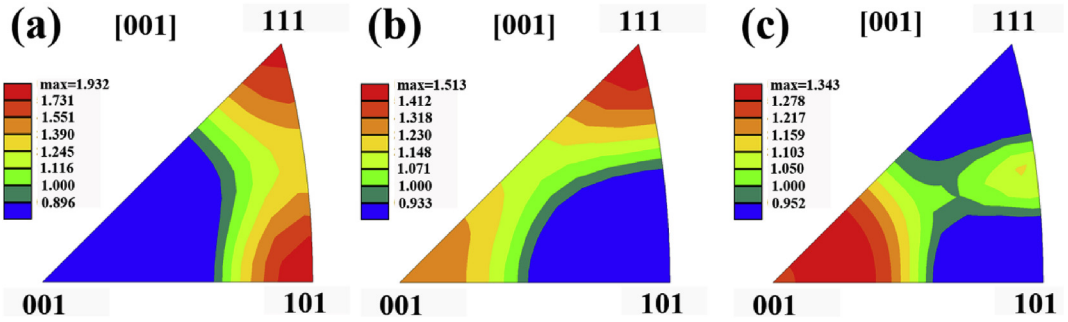

Fig. 3. Inverse pole figures of (a) T6 7055, (b) FSP 7055, and (c) FSP+T6 7055.

with size of approximately 10 nm (identified by selected diffraction area and dark field (DF) image) were obtained in the T6 7055 + 0.25Sc sample, and some of the $Al_3(Sc,Zr)$ particles were located in the GBs (Fig. 6(d)).

The precipitates in the FSP samples were characterized by larger size and lower density as compared to the precipitates in the T6 samples. Thus, Sc addition could reduce the size and increase the density of the precipitated phase in the FSP samples (Fig. 6(b) and (e)). The DF image obtained using the reflection of $Al_3(Sc,Zr)$ phase confirmed that the nanoparticles in the large precipitated phase in the FSP 7055 + 0.25Sc sample were $Al_3(Sc,Zr)$ (Fig. 6(e)).

T6 treatment decreased the density of large precipitates in the FSP samples, and a high density of precipitates with several nanometres was obtained in the two FSP+T6 samples (Fig. 6(c) and (f)). Similar to the 7xxx alloys with conventional T6 treatment, a precipitation-free zone (PFZ) was also observed in the FSP samples after the T6 process (Fig. 6(c)). $Al_3(Sc,Zr)$ particles were also found in the FSP+T6 7055 + 0.25Sc sample (Fig. 6(f)).

Fig. 7 depicts the stress–strain curves for the 7055 and 7055 + 0.25Sc alloys, and Table 1 shows the mechanical properties. The 7055 + 0.25Sc alloy exhibited higher strength than the 7055 alloy with the same state. For the alloy with the same components, the FSP sample exhibited lower strength than the T6 sample, and the additional T6 treatment could improve the strength of the FSP sample. The yield strength (YS) and UTS of the FSP 7055 + 0.25Sc sample after T6 process reached 592 and 636 MPa, respectively.

Fig. 8 shows the temperature-dependent internal friction (TDIF) for the 7055 and 7055 + 0.25Sc alloys. The IF value of all samples generally increased with the increasing temperature. For the 7055 alloy, the FSP sample exhibited higher IF increase rate and greater high-temperature (higher than 460 K) IF value than the T6 sample, and FSP+T6 sample exhibited the lowest high-temperature IF value. The peaks at 450 and 475 K were observed in the TDIF curves for the T6 and FSP samples, respectively (Fig. 8(a)). For the 7055 + 0.25Sc alloy, the FSP sample also exhibited the highest IF increase rate and high-temperature IF value, but the T6 treatment did not greatly reduce the IF value of FSP sample. Moreover, the FSP+T6 sample exhibited greater high-temperature IF value than the T6 sample. The IF peak at 475 K was observed in the TDIF curve for FSP 7055 + 0.25Sc sample (Fig. 8(b)).

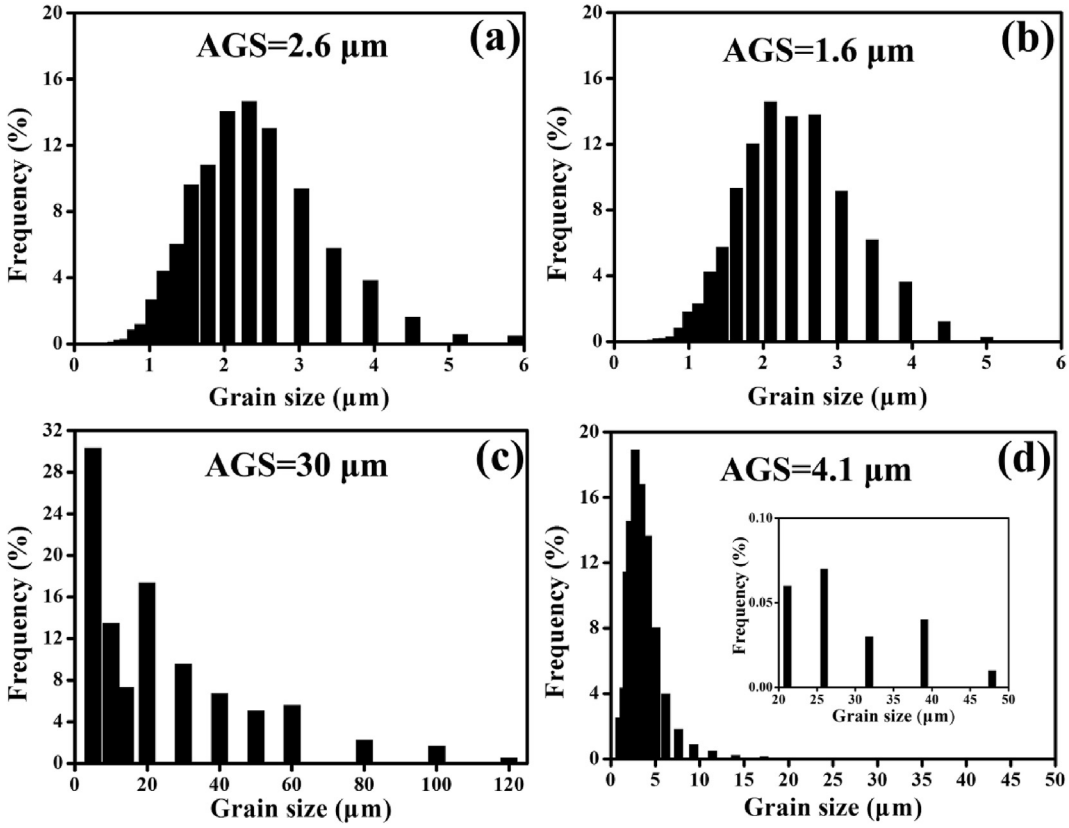

Fig. 4. Grain size distributions for (a) FSP 7055, (b) FSP 7055 + 0.25Sc, (c) FSP+T6 7055, and (d) FSP+T6 7055 + 0.25Sc samples.

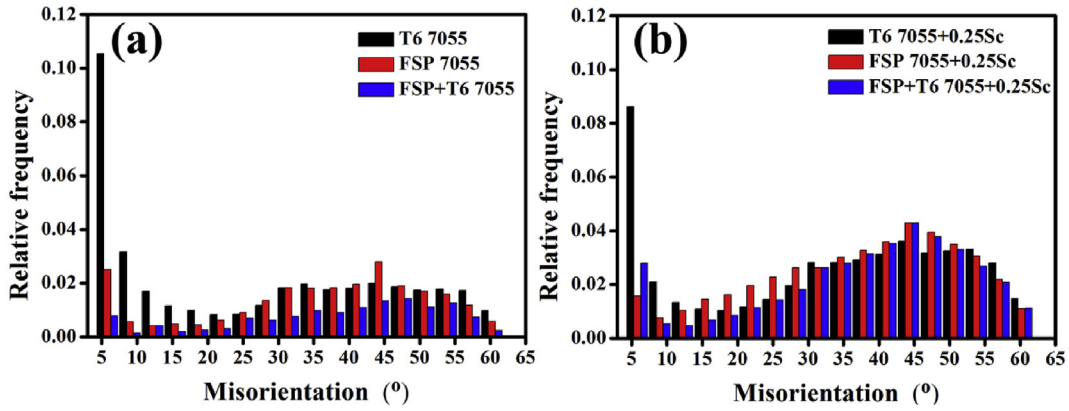

Fig. 5. Misorientation angle distributions of (a) 7055 and (b) 7055 + 0.25Sc samples.

4. Discussion

The T6 7055 + 0.25Sc sample showed finer grains than the T6 7055 sample (Fig. 2(a) and (d)). The $Al_3(Sc,Zr)$ phase exhibited GB pinning effect in the Sc-containing Al alloy [16–20], and some of $Al_3(Sc,Zr)$ particles were also found in the GBs of the T6 7055 + 0.25Sc sample. Thus, the recrystallization and the growth of recrystallized grains in the 7055 + 0.25Sc alloy during T6 process were inhibited by the $Al_3(Sc,Zr)$ particles, and more deformed grains with a fibrous structure were retained in this sample.

The grain growth of 7055 + 0.25Sc alloy during FSP could also be inhibited by the $Al_3(Sc,Zr)$ particles. Thus, the AGS of the FSP 7055 + 0.25Sc sample was finer than that of the FSP 7055 sample (Fig. 2(b) and (e)).

The precipitation process and the grain size of the FSP sample were affected by Sc addition. The standard precipitation sequence for 7xxx Al alloys is: supersaturated solid solution → clusters → GP zones → η′ → η (Zn_2Mg). FSW or FSP leads to η phase precipitation in the stirred zone of 7xxx Al alloys [29,30]. η phase with a large size was also found in the FSP 7055 and 7055 + 0.25Sc samples (Fig. 6(b) and (e)). For the 7055 + 0.25Sc alloy, the $Al_3(Sc,Zr)$ particles could provide heterogeneous nucleation sites, thereby enhancing the precipitation efficiency during FSP. Thus, the FSP 7055 + 0.25Sc sample exhibited a higher density and finer η phase than the FSP 7055 sample. In addition, some of the $Al_3(Sc,Zr)$ particles were found in the η phase in the FSP 7055 + 0.25Sc sample (Fig. 6(b) and (e)).

Solid-solution treatment led to stable η phase dissolution, and

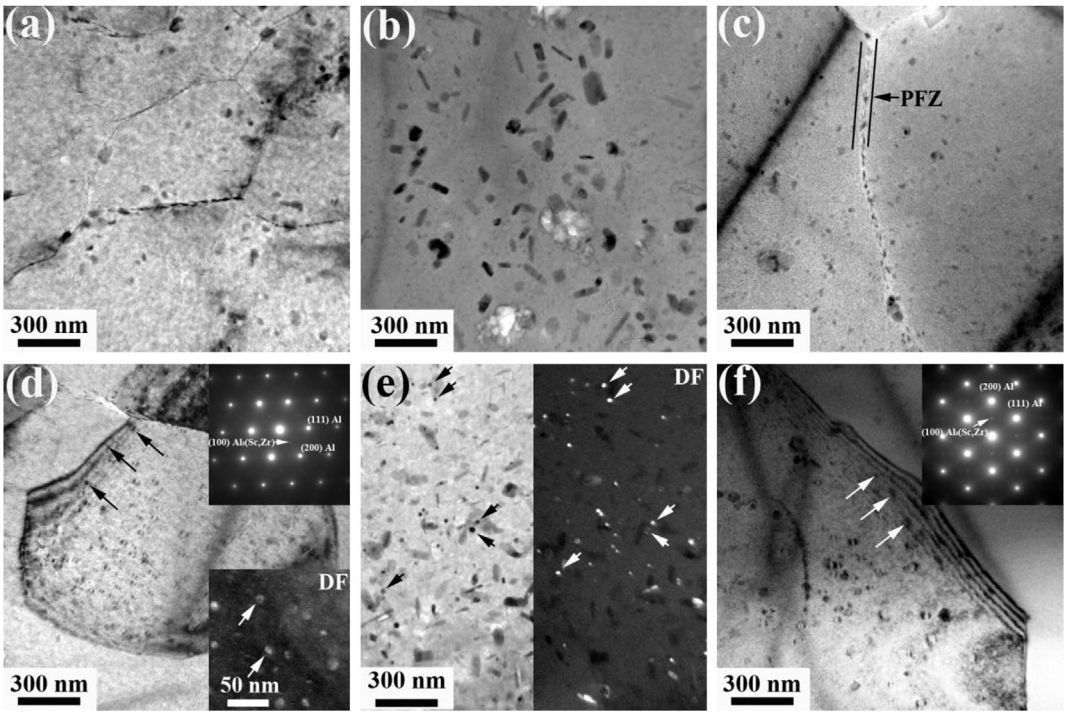

Fig. 6. TEM images of (a) T6 7055, (b) FSP 7055, (c) FSP+T6 7055, (d) T6 7055 + 0.25Sc, (e) FSP 7055 + 0.25Sc, and (f) FSP+T6 7055 + 0.25Sc samples. The arrows in panel (d–f) denote the $Al_3(Sc,Zr)$ phase.

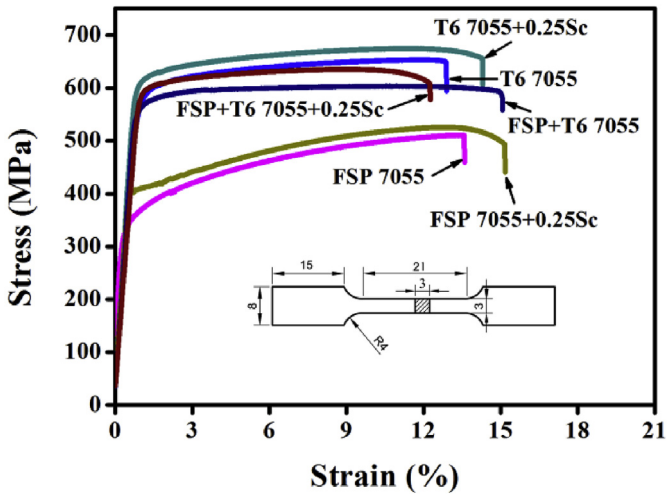

Fig. 7. Stress–strain curves of 7055 and 7055 + 0.25Sc samples.

the subsequent aging led to precipitation of the metastable η′ phase. Thus, a high density of η′ with size of several nanometres was obtained in the FSP+T6 samples (Fig. 6(c) and (f)). The AGS for FSP 7055 increased to 30 μm after T6 treatment, while the coarsening of grain in the FSP 7055 + 0.25Sc sample during T6 process was effectively inhibited by the Sc addition due to the boundary pinning effect of the $Al_3(Sc,Zr)$ phase. Thus, a low proportion of large grains was obtained in the FSP+T6 7055 + 0.25Sc sample (Fig. 4(d)). However, the distribution of $Al_3(Sc,Zr)$ particles was non-uniform, which led to the local abnormal grain growth in the FSP 7055 + 0.25Sc sample during the T6 process. Thus, the FSP+T6 7055 + 0.25Sc sample exhibited a multi-scale equiaxed grain structure (Figs. 2(f) and 4(d)).

FSP is an important severe plastic deformation (SPD) method usually used to refine grains of metal [11,31,32]. However, compared with the 7xxx alloys fabricated by other SPD methods such as equal channel angular pressing [33], high pressure torsion [34], and cryorolling [35], the FSP samples exhibited lower hardness and strength (Figs. 1 and 7). In addition to grain coarsening and dislocation annihilation, the transformation of η′ into η phase also occurred in the 7xxx Al alloys during FSP owing to the severe friction induced by the increase in temperature. The lower GB, dislocation, and precipitation strengthening led the lower hardness and strength of the FSP 7xxx than those of the 7xxx Al alloy which underwent other SPD processes. Furthermore, the precipitation of stable η phase also led to the lower strength of the FSP samples than the T6 samples in this study and the 7055 alloy with simple

Table 1
Tensile properties of 7055 and 7055 + 0.25Sc samples.

Sample		YS (MPa)	UTS (MPa)	EL (%)
T6	7055	577	654	13
	7055 + 0.25Sc	600	679	14
FSP	7055	337	510	13
	7055 + 0.25Sc	436	560	15
FSP+T6	7055	568	600	15
	7055 + 0.25Sc	592	636	12

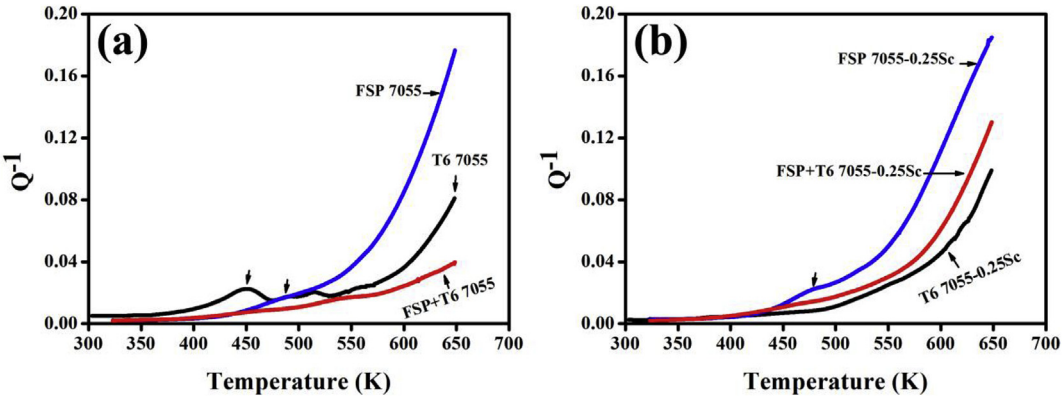

Fig. 8. TDIF curves of (a) 7055 and (b) 7055 + 0.25Sc samples.

thermomechanical treatment [36].

Precipitates tend to nucleate preferentially in the GBs in Al alloys during artificial aging [37]. Compared with the samples without FSP, more GBs were obtained in the FSP samples due to the lower grain size. Thus, the FSP samples exhibited a higher efficiency of precipitation and the a much shorter peak-aged time than the samples without FSP (Fig. 1).

T6 treatment led to the precipitation of metastable η′ phase in the FSP samples, thereby improving the strength of FSP samples (Fig. 7 and Table 1). However, for the alloy with the same components, the hardness and UTS of the FSP+T6 sample were lower than those of T6 samples. The coarse grains in the FSP+T6 7055 weakened the GB strengthening, and thus the FSP+T6 7055 alloy exhibited lower strength than the T6 7055 alloy. The T6 7055 + 0.25Sc alloy did not exhibit lower grains size than the FSP+T6 7055 + 0.25Sc alloy (Fig. 2), but this sample showed a stronger ⟨111⟩ texture than the FSP+T6 7055 + 0.25Sc (Fig. 3). *Hou et* al. showed that the strong ⟨111⟩ texture could improve the strength of Al alloy [38]. Thus, the weak ⟨111⟩ texture resulted in lower strength of FSP-preceded 7055 + 0.25Sc alloy compare with the conventional T6 treatment. Compared with the 7055 alloy, the 7055 + 0.25Sc alloy with the same processing route exhibited higher strength due to the higher GB strengthening effect due to the finer grains.

Characteristic peaks were observed in the TDIF curves of the T6 7055 and FSP 7055 and FSP 7055 + 0.25Sc samples. Previous researchers found that the peaks around 450 K in the TDIF curves of Al materials are associated with the viscous sliding along the GBs [39–42]. The excellent GB sliding capacities of the FSP Al alloys at high temperature can be attributed to the fine grains and high fraction of high misorientation angle [22,23,26]. In the present study, the FSP 7055 and 7055 + 0.25Sc alloys also showed the above structural characteristics (Figs. 2, 4 and 5). Thus, the peaks caused by GB relaxation were observed in the TDIF curves of the two FSP samples.

The T6 and FSP+T6 7055 + 0.25Sc samples were subjected to high-temperature treatment for a long time (743 K/2 h), and the GBs of these two samples were pinned by nanometre-sized Al_3(Sc,Zr) (Fig. 6d and f). *Golovin et* al. showed that the GB pinning phase could suppress the GB IF in the Al alloys [43,44]. Thus, the peaks were absent in the TDIF curves of the T6 and FSP+T6 7055 + 0.25Sc samples. Compared with the FSP+T6 7055 alloy, the T6 7055 alloy contained much more fine recrystallized grains (Fig. 2a and c), which could promote grain sliding of 7xxx alloys during high-temperature deformation [45]. Thus, the peak was observed in the TDIF curve of the T6 7055 alloy, but absent in the curve of the FSP+T6 7055 alloy.

The IF value of all samples generally increased with increasing temperature (Fig. 8). The high-temperature damping can be explained by dislocation damping and GB damping mechanisms [46]. The number of point defects increases with the increase in temperature during vibration, and the IF value is mainly controlled by vacancies [47,48]. GB slipping is another important contributor to the increase in IF during high-temperature vibration. With the increase in temperature, GB sliding dissipates more elastic energy, which then increases the IF value [49].

In this study, the FSP promoted the precipitation of Zn and Mg atoms, and then led to the transformation of η′ phase with high density and tiny size into η phase with low density and large size (Fig. 6b and e). Thus, the number of pinning points, which could hinder the motion of dislocations, was decreased, and then the IF value of sample increased after FSP. Furthermore, the smaller grain size of FSP samples increased the GB area of the FSP samples, resulting in greater energy that can be dissipated in these samples during vibration at high temperature, according to the GB damping mechanisms [46,49]. Thus, the FSP samples exhibited the greatest high-temperature IF value.

The PFZ with lower density of solute atom and precipitate was obtained in the 7xxx Al alloys after aging treatment (Fig. 6(c)). The FSP+T6 7055 + 0.25Sc sample contained larger area of PFZ than the other three samples that underwent T6 treatment due to the finer grains. Thus, the pinning points in the FSP+T6 7055 + 0.25Sc sample were lower than the other three samples during high-temperature vibration. In addition, this sample exhibited greater high-temperature IF value than the 7055 sample that underwent the same process and the T6 samples. The FSP+T6 7055 + 0.25Sc sample also showed high fraction of high misorientation angle and fine grains (Fig. 5), which could improve the GB slipping; this structure may also improve the IF value of the sample according to the GB damping mechanism [49].

5. Conclusions

The damping and mechanical properties of 7055 Al alloy after Sc addition, FSP, and T6 treatment were investigated. The conclusions are summarized as follows:

(1) The T6 samples exhibited higher strength than the FSP samples. Further T6 treatment could lead to dissolution of η phase and precipitation of η′ phase in the FSP samples, thereby improving their mechanical properties. Sc addition could improve the mechanical properties of 7055 alloys subjected to any process.

(2) The greater high-temperature IF value of the FSP sample than the other samples can be attributed to the low density of solute atom and precipitate phase, as well as the fine equiaxed grain structure. The peaks in the TDIF curves of the two FSP samples were caused by GB relaxation.
(3) The Al_3(Sc,Zr) phase inhibited the grain growth of the FSP 7055 + 0.25Sc sample during additional T6 process. A high density of metastable η′ phase and fine grains with high fraction of high misorientation angle were obtained in the FSP+T6 7055 + 0.25Sc sample. This structure led resulted in the balanced properties of the FSP+T6 7055 + 0.25Sc sample, including large high-temperature IF value and reasonable mechanical properties.

Acknowledgements

This work was funded by the National Natural Science Foundation of China (No.51601045), the Guangxi "Bagui" Teams for Innovation and Research, the Guangxi Natural Science Foundation (No. 2016GXNSFDA380028), and the Science and Technology Major Project of Guangxi (No. GKAA17202007).

Appendix A. Supplementary data

Supplementary data to this article can be found online at https://doi.org/10.1016/j.jallcom.2018.09.109.

References

[1] X.S. Hu, Y.K. Zhang, M.Y. Zheng, K. Wu, Scr. Mater. 52 (2005) 1141–1145.
[2] M.C. Gui, D.B. Wang, J.J. Wu, G.J. Yuan, C.G. Li, Mater. Sci. Eng. A 286 (2000) 282–288.
[3] D.R. Ni, J.J. Wang, Z.Y. Ma, J. Mater. Sci. Technol. 32 (2016) 162–166.
[4] N. Srikanth, H.K.F. Calvin, M. Gupta, Mater. Sci. Eng. A 423 (2006) 189–191.
[5] H.J. Jiang, C.Y. Liu, Y. Chen, Z.X. Yang, H.F. Huang, L.L. Wei, Y.B. Li, H.Q. Qi, J. Alloys Compd. 739 (2018) 114–121.
[6] B.H. Luo, Z.H. Bai, Y.Q. Xie, Mater. Sci. Eng. A 370 (2004) 172–176.
[7] Z.H. Ma, F.S. Han, J.N. Wei, J.C. Gao, Metall. Mater. Trans. A 32 (2000) 2657–2661.
[8] H.J. Jiang, C.Y. Liu, Z.Y. Ma, X. Zhang, L. Yu, M.Z. Ma, R.P. Liu, J. Alloys Compd. 722 (2017) 138–144.
[9] J.N. Wei, D.Y. Wang, W.J. Xie, J.L. Luo, F.S. Han, Phys. Lett. A 366 (2007) 134–136.
[10] W.M. Thomas, E.D. Nicholas, J.C. Needham, M.G. Murch, P. Templesmith, C.J. Dawes, Friction Stir Butt Welding, GB Patent Application (1991) No. 9125978.8.
[11] R.S. Mishra, Z.Y. Ma, Mater. Sci. Eng. R 50 (2005) 1–78.
[12] G.K. Padhy, C.S. Wu, S. Gao, J. Mater. Sci. Technol. 34 (2018) 1–38.
[13] H.J. Jiang, C.Y. Liu, B. Zhang, P. Xue, Z.Y. Ma, K. Luo, M.Z. Ma, R.P. Liu, Mater. Char. 131 (2017) 425–430.
[14] Y. Chen, C.Y. Liu, B. Zhang, Z.Y. Ma, W.B. Zhou, H.J. Jiang, H.F. Huang, L.L. Wei, Mater. Char. 135 (2018) 25–31.
[15] Y.Q. Mao, L.M. Ke, Y.H. Chen, F.C. Liu, L. Xing, J. Mater. Sci. Technol. 34 (2018) 228–236.
[16] G.B. Teng, C.Y. Liu, Z.Y. Ma, W.B. Zhou, L.L. Wei, Y. Chen, J. Li, Y.F. Mo, Mater. Sci. Eng. A 713 (2018) 61–66.
[17] C.Y. Liu, H.J. Jiang, B. Zhang, Z.Y. Ma, Mater. Char. 136 (2018) 382–387.
[18] B.A. Chen, L. Pan, R.H. Wang, G. Liu, P.M. Cheng, L. Xiao, J. Sun, Mater. Sci. Eng. A 530 (2011) 607–617.
[19] L. Jiang, J.K. Li, G. Liu, R.H. Wang, B.A. Chen, J.Y. Zhang, J. Sun, M.X. Yang, G. Yang, J. Yang, X.Z. Cao, Mater. Sci. Eng. A 637 (2015) 139–154.
[20] G. Li, N.Q. Zhao, T. Liu, J.J. Li, C.N. He, C.S. Shi, E.Z. Liu, J.W. Sha, Mater. Sci. Eng. A 617 (2014) 219–227.
[21] J.H. Kim, J.H. Kim, J.T. Yeom, D.G. Lee, S.G. Lim, N.K. Park, J. Mater. Process. Technol. 187–188 (2007) 635–639.
[22] F.C. Liu, Z.Y. Ma, F.C. Zhang, J. Mater. Sci. Technol. 28 (2012) 1025–1030.
[23] F.C. Liu, Z.Y. Ma, L.Q. Chen, Scr. Mater. 60 (2009) 968–971.
[24] Y. Deng, B. Peng, G.F. Xu, Q.L. Pan, Z.M. Yin, R. Ye, Y.J. Wang, L.Y. Lu, Mater. Sci. Eng. A 639 (2015) 500–513.
[25] I. Charita, R.S. Mishraba, J. Mater. Sci. Technol. 34 (2018) 214–218.
[26] F.C. Liu, Z.Y. Ma, Scr. Mater. 59 (2008) 882–885.
[27] M.S. Blanter, I.S. Golovin, H. Neuhäuser, H.-R. Sinning, Internal Friction in Metallic Materials, a Handbook, Springer, Berlin Heidelberg New York, 2007.
[28] I.S. Golovin, V.V. Palacheva, V.Yu. Zadorozhnyy, J. Zhu, H. Jiang, J. Cifre, T.A. Lograsso, Acta Mater. 78 (2014) 93–102.
[29] A. Orozco-Caballero, P. Hidalgo-Manrique, C.M. Cepeda-Jiménez, P. Rey, D. Verdera, O.A. Ruano, F. Carreño, Mater. Char. 112 (2016) 197–205.
[30] Y. Chen, H. Ding, Z.H. Cai, J.W. Zhao, J.Z. Li, Mater. Sci. Eng. A 650 (2016) 396–403.
[31] Y.T. Zhu, X.Z. Liao, Nat. Mater. 3 (2004) 351–352.
[32] S.V. Divinski, G. Reglitz, I.S. Golovin, M. Peterlechner, R. Lapovok, Y. Estrin, G. Wilde, Acta Mater. 82 (2015) 11–21.
[33] C.M. Cepeda-Jiménez, J.M. García-Infanta, O.A. Ruano, F. Carreño, J. Alloys Compd. 509 (2011) 8649–8656.
[34] K.S. Ghosh, N. Gao, M.J. Starink, Mater. Sci. Eng. A 552 (2012) 164–171.
[35] S.K. Panigrahi, R. Jayaganthan, J. Alloys Compd. 509 (2011) 9609–9616.
[36] J.R. Zuo, L.G. Hou, J.T. Shi, H. Cui, L.Z. Zhuang, J.S. Zhang, J. Alloys Compd. 716 (2017) 220–230.
[37] C.Y. Liu, M.Z. Ma, R.P. Liu, K. Luo, Mater. Sci. Eng. A 654 (2016) 436–441.
[38] J.P. Hou, R. Li, Q. Wang, H.Y. Yu, Z.J. Zhang, Q.Y. Chen, H. Ma, X.M. Wu, X.W. Li, Z.F. Zhang, J. Alloys Compd. 769 (2018) 96–109.
[39] T.S. Kê, Phys. Rev. 71 (1947) 533–546.
[40] B. Cai, Q.P. Kong, P. Cui, H.T. Cong, X.K. Sun, Scripta Mater. 44 (2001) 1043–1048.
[41] Q.P. Kong, W.B. Jiang, Y. Shi, P. Cui, Q.F. Fang, M. Winning, Mater. Sci. Eng. A 521–522 (2009) 128–133.
[42] A. Al Sadi, E. Bonetti, P. Mattioli, G. Valdre, J. Alloys Compd. 211 (1994) 489–493.
[43] I.S. Golovin, A.S. Bychkov, A.V. Mikhailovskaya, S.V. Dobatkin, Phys. Met. Metallogr. 115 (2014) 192–201.
[44] I.S. Golovin, A.V. Mikhaylovskaya, H.-R. Sinning, J. Alloys Compd. 577 (2013) 622–632.
[45] K. Wang, F.C. Liu, Z.Y. Ma, F.C. Zhang, Scripta Mater. 64 (2011) 572–575.
[46] S.Q. Chen, X.P. Dong, R. Ma, L. Zhang, H. Wang, Z.T. Fan, Mater. Sci. Eng. A 551 (2012) 87–94.
[47] M. Yamaguchi, J. Bernhardt, K. Faerstein, D. Shtansky, Y. Bando, I.S. Golovin, H.R. Sinning, D. Golberg, Acta Mater. 61 (2013) 7604–7615.
[48] A.V. Mikhaylovskaya, V.K. Portnoy, A.G. Mochugovskiy, M.Yu. Zadorozhnyy, N.Yu. Tabachkova, I.S. Golovin, Mater. Des. 109 (2016) 197–208.
[49] J. Zhang, R.J. Perez, E.J. Lavernia, J. Mater. Sci. 28 (1993) 2395–2404.